Indian Journal of Chemical Technology
Vol. 31, July 2024, pp. 593-603
DOI: 10.56042/ijct.v31i4. 7530

Computational analysis for magnetized radiative Jeffrey nanofluid ($Au/C_2H_6O_2$) flow in a rotating system with activation energy

K. Kumaraswamy Naidu[1], D. Harish Babu[2], P.V. Satya Narayana[3]*, S. Harinath Reddy[4] & A.M. Rashad[5]

[1]Dept. of Mathematics, Mohan Babu University (Erstwhile Sree Vidyanikethan Engg. Coll.), Tirupati-517 102, A.P, India

[2]Dept. of Mathematics, SASL, VIT Bhopal University, Bhopal-466114, M P, India

[3]Dept. of Mathematics, SAS, Vellore Institute of Technology, Vellore – 632 014, T.N, India

[4]Dept. of Mathematics, Annamacharya Inst. of Tech. and Sci., Rajampet, A.P, India

[5]Department of Mathematics, Aswan University, Faculty of Science, Aswan, 81528, Egypt

*E-mail: pvsatya8@yahoo.co.in

Received 24 December 2023; accepted 27 May 2024

The current paper is aimed at investigating the impact of Arrhenius energy and thermal radiation on a Jeffrey nanoliquid using the Tiwari-Das model within a rotating porous system. The study includes *Au*, (Gold) as a nanoparticle, and ethylene glycol (EG) as a base fluid. The leading partial differential equations describing the flow are formulated based on the general laws of momentum, energy and species concentrations. The applicable dimensionless configuration reduces the complexity of the flow model, allowing it to be solved numerically. The Runge-Kutte Fehlberg scheme, in concert with MATLAB, is used to solve the transformed equations. Multiple graphs and tables are used to examine the new results comprehensively regarding fundamental flow, magnetic, and thermal properties for various implanted parameters. It is observed that the concentration profile seems higher for progressive values of Arrhenius energy, whereas the opposite behaviour has been observed for greater values of the Schmidt number and chemical reaction parameter. The findings from this research can be applied to the development of many technologies such as solar power plants, nanofluidic devices, micro pumps, etc.

Keywords: Activation energy, Chemical reaction, Jeffrey fluid, Rotating system, Thermal radiation, Tiwari-Das nanofluid model

Introduction

Recent advances in technology have been greatly influenced by nanoparticles, particularly in their capacity to facilitate the transport of mass and heat. In view of this, nanoliquids are considered. However, nanofluids are a subclass of liquid composed of particles measuring between 1 and 100 nm. The colloidal particles of nanomaterial (*Au)* are suspended in the base fluid Ethylene Glycol (EG). Several academics have expressed an interest in learning the flow of these nanoliquids across varied geometries under the impact of a variety of variables. It has already been demonstrated that including nanoparticles in the fluids used in solar processes can significantly increase the efficiency of those processes, which in turn makes them the most effective. In cooling and heating applications, nanofluids frequently play a crucial role. Poply and Vinita[1] conducted research to determine how the results of thermal flux and heat production affect the heat transmission rate of a nanoliquid over a stretched cylinder. Sheikholeslami and Ganji[2] studied the effect of thermal conduction using a two-phase nanoliquid model in a rotating system. They reported that the temperature boundary layer becomes thicker as the Brownian motion and thermophoresis parameters increase. Rashidi *et al*.[3] looked at how the second law of thermodynamics applies to the motion of a nanoliquid that is both electrically conductive and incompressible over a porous, spinning disc. They concluded that magnetic spinning disc drives could have major consequences for improving heat transfer in renewable energy systems. Non-Newtonian nanofluids flowing through a conduit are addressed by Ellahi[4]. They considered two thermal viscosity models. Even with a wide range of viscosities, he found that fluid motion is slowed by the MHD parameter. Ali *et al*.[5] discussed the heat and mass transfer of a nanoliquid inside deformed parallel walls. Santhosh and Sivaraj[6] analysed the impact of

thermal radiation on the mixed convective heat transfer of a viscous nanofluid in a porous cavity. Vijayalakshmi and Sivaraj[7] studied the heat transfer analysis of micropolar nanofluid in an inclined square cavity with magnetic and radiation effects. Sharma *et al*.[8] studied the motion of viscous nanofluid over a rotating disk with viscous dissipation moving upward/downward. Kumar *et al*.[9] studied the impact of entropy generation in water conveying nanoparticles flow over a vertically rotating surface. Numerous studies[10–13] analyzed the impact of mass and heat movement on nanoliquids with different geometries.

The activation energy of a substance is the minimum quantity of energy it needs to possess in order to undergo a chemical reaction or transformation. Several issues related to geothermal and gasoline distribution technologies were identified as critical, including species compound changes with limited Arrhenius inception. To analyse the impact of enactment essentiality on streams, it is essential to produce speculative outcomes as opposed to using test methods. Sometimes, geothermal production, oil reserves, engineering technologies and agricultural production can benefit from activation energy. The activation energy behavior of binary processes in a convective flow within a porous media was explored in detail by Bestman[14]. The rheology of non-Newtonian fluids on rotating surfaces was studied by Khan *et al*.[15], who focused on the effects of electromagnetic and Arrhenius energy. Muhammad *et al*.[16] assessed the numerical modelling of Eyring-Powell nanoliquid and nonlinear thermal radiation in three-dimensional flow. Radiation and activation energy's impact on the accelerated flow of a secondary fluid were investigated by Khan *et al*.[17] using nanomaterials. An increase in the Lewis parameter reduces the Casson nanoliquid concentration distribution, as shown by Gireesha *et al*.[18]. Other pertinent studies are presented in other literatures[19-22].

Although most industrial and organic liquids are non-Newtonian and Newton's equation of viscosity cannot completely capture their intricate rheological features, little research has been done on how they flow through porous-walled channels. Non-Newtonian fluid models are often used in the study of physiological liquids, and the Jeffrey liquid model is one of them. The Jeffrey liquid model, as opposed to the viscous liquid model, might be a representation of fluid stress relaxation that is not Newtonian. In order to show how free convection impacts the peristaltic movement of Jeffrey liquid in a constrained vertical porous layer studied by Vajravelu *et al*.[23]. In a composite horizontal channel made of a deformable porous material, Naidu and Sreenadh[24] investigated the Poiseuille flow of a non-Newtonian Jeffrey liquid. Numerous researchers[25-27] studied the impact of various physical parameters on fluid flow by considering the single Jeffrey fluid parameter. A nonlinear stretching surface that causes the flow of Jeffrey nanoliquid under both zero and nonzero normal mass flux conditions was examined by Hayat *et al*.[28]. Shahzad *et al*.[29] studied the computational characterization of thermal and electrically conducting flows of a Jeffrey nanoliquid across a stretching surface with Joule heating and viscous dissipation using single phase nanoliquid model. Harish and Satyanarayana[30] looked into the MHD heat transfer of an incompressible Jeffrey liquid through an expanding porous sheet subjected to a power law heat flux and joule heating. They demonstrated that the Deborah number has a major impact on the thickness of the momentum and thermal boundary layers. Zeeshan and Majid[31] studied heat transfer analysis of non-Newtonian Jeffrey fluid over an elongated sheet with magnetic dipole impact. Many researchers[32-35] looked at the impact of various physical pertinent parameters on Jeffrey fluid flow (two Parameters)in a variety of geometries.

According to our review of the pertinent literature, the current problem of evaluating the mass and heat transmit effects of Jeffrey nanoliquid using the Tiwari Das model[36] in a revolving system with activation energy has not yet been addressed. Hence the magnetohydrodynamic Jeffrey nanofluid flow in a channel with thermal radiation and activation energy is studied in the present analysis. The flow equations are reduced to dimensionless form, and numerical results are obtained using the MATLAB-implemented Runge-Kutta Fehlberg method. Lastly, a graphical depiction of the impact of various physical factors on the momentum and temperature profiles is displayed. The present study has various applications like chemical processing, biomedical engineering applications, electronic cooling systems, solar energy systems, heat exchangers and nanotechnology. To assess the accuracy of the present data, we compared them to previously published results, which supported our study.

Modelling

The three-dimensional steady flow of electrical conducting single-phase nanoliquid among two

horizontal parallel plates $y=0$ to $y=h$ is considered when the plate and liquid rotate together around the axis perpendicular to the plate and rotates at a constant angular velocity, and it is represented in Fig. 1. In the coordinate system, the x-axis is parallel to the plate and the flow is in equilibrium; the y-axis is orthogonal and the z-axis is normal to the xy-plane. Finally, we consider the subsequent assumptions:

1. The induced magnetic field is neglected due to low Reynolds number.
2. Gold (Au) nanoparticle is considered as a nanofluid and Ethylene Glycol (EG) as base fluid.
3. The upper plate is constantly being injected or sucked by the wall at a constant velocity $v_0 > 0$ or $v_0 < 0$. Constant cold (T_0) and hot (T_h) temperatures are maintained on the upper and lower plates, respectively.
4. Jeffrey fluid is incorporated due to its simplicity amongst non-Newtonian fluids.
5. The radiation and Heat sources are mainly focused on a Temperature gradient.
6. Activation energy is regarded in Mass fraction.

The governing equations for a rotating frame based on these postulations and the nanoliquid model presented by the literatures[36, 37, 38] are as follows.

$$\frac{\partial u}{\partial x}+\frac{\partial v}{\partial y}+\frac{\partial w}{\partial z}=0. \quad \text{... (1)}$$

$$\left(u\frac{\partial u}{\partial x}+v\frac{\partial u}{\partial y}\right)+2\Omega w=-\frac{1}{\rho_{Nf}}\frac{\partial p}{\partial x}+\frac{\vartheta_{Nf}}{1+\lambda}\left(\frac{\partial^2 u}{\partial x^2}+\frac{\partial^2 u}{\partial y^2}\right)-\left(\frac{\sigma B_0^2 u}{\rho_{Nf}}+\frac{\vartheta_{Nf}}{k_0}u\right) \quad \text{... (2)}$$

$$\left(u\frac{\partial v}{\partial y}\right)=-\frac{1}{\rho_{Nf}}\frac{\partial p}{\partial y}+\frac{\vartheta_{Nf}}{1+\lambda}\left(\frac{\partial^2 v}{\partial x^2}+\frac{\partial^2 v}{\partial y^2}\right). \quad \text{... (3)}$$

$$\left(u\frac{\partial w}{\partial x}+v\frac{\partial w}{\partial y}\right)-2\Omega u=\frac{\vartheta_{Nf}}{1+\lambda}\left(\frac{\partial^2 w}{\partial x^2}+\frac{\partial^2 w}{\partial y^2}\right)-\left(\frac{\sigma B_0^2 w}{\rho_{Nf}}+\frac{\vartheta_{Nf}}{k_0}w\right) \quad \text{... (4)}$$

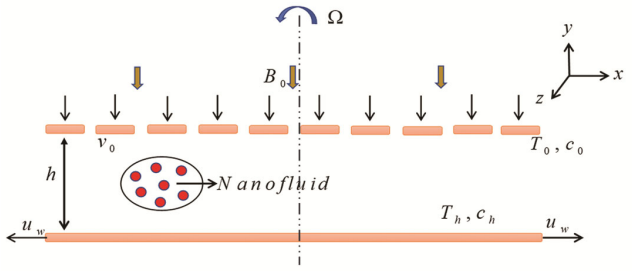

Fig. 1 — Flow Diagram

$$\left(u\frac{\partial T}{\partial x}+v\frac{\partial T}{\partial y}+w\frac{\partial T}{\partial z}\right)=\alpha_{Nf}\left(\frac{\partial^2 T}{\partial x^2}+\frac{\partial^2 T}{\partial y^2}+\frac{\partial^2 T}{\partial z^2}\right)-\frac{1}{\left(\rho C_p\right)_{Nf}}\frac{\partial q_r}{\partial y}+\frac{1}{\left(\rho C_p\right)_{Nf}}Q_0(T-T_0) \quad \text{... (5)}$$

$$\left(u\frac{\partial c}{\partial x}+v\frac{\partial c}{\partial y}+w\frac{\partial c}{\partial z}\right)=D\left(\frac{\partial^2 c}{\partial x^2}+\frac{\partial^2 c}{\partial y^2}+\frac{\partial^2 c}{\partial z^2}\right)-Kr^2(c-c_0)\left(\frac{T}{T_0}\right)^m e^{-\left(\frac{Ea}{k^*T}\right)} \quad \text{... (6)}$$

with boundary conditions[37]

$$u=ax, v=w=0, T=T_h, c=c_h \text{ at } y=0. \quad \text{... (7)}$$

$$u=w=0, v=v_0, T=T_0, c=c_0 \text{ at } y=h. \quad \text{... (8)}$$

Similarity revolt [37]

$$\eta=\frac{y}{h}, u=axf'(\eta), v=-ahf(\eta), w=axg(\eta), \theta(\eta)=\frac{T-T_0}{T_h-T_0}, \phi(\eta)=\frac{c-c_0}{c_h-c_0} \quad \text{... (9)}$$

By plugging Eq. (9) into Eqs (1)-(4) and dropping the pressure gradient terms, the following equations are derived.

$$f'''(\eta)+(1+\lambda)\frac{A_2}{A_1}\left(\mathrm{Re}\left[f'^2(\eta)-f(\eta)f''(\eta)\right]\right)+2(1+\lambda)\frac{A_2}{A_1}Rpg(\eta)-(1+\lambda)\frac{A_2}{A_1}.\left[\frac{M^2}{A_2}+\frac{A_1K}{A_2}\right]f'(\eta)=A \quad \text{... (10)}$$

where A is constant and Differentiate Eq.(10) w.r.to η, then we get

$$f''''(\eta)+(1+\lambda)\frac{A_2}{A_1}\left(\mathrm{Re}\left[f'(\eta)f''(\eta)-f(\eta)f'''(\eta)\right]\right)+2(1+\lambda)\frac{A_2}{A_1}Rpg'(\eta)-(1+\lambda)\frac{A_2}{A_1}.\left[\frac{M^2}{A_2}+\frac{A_1K}{A_2}\right]f''(\eta)=0 \quad \text{... (11)}$$

$$g''(\eta)-(1+\lambda)\frac{A_2}{A_1}\left(\mathrm{Re}\left[f(\eta)\,g'(\eta)-f'(\eta)\,g(\eta)\right]\right)+2(1+\lambda)Rp\frac{A_2}{A_1}f'(\eta)-(1+\lambda)\frac{A_2}{A_1}\left[\frac{M^2}{A_2}+\frac{A_1K}{A_2}\right]g(\eta)=0 \quad \text{... (12)}$$

Also, by substituting (9) into (5)-(6) then we get the following equations

$$(A_3+Rd)\theta''(\eta)+A_4\,\mathrm{Pr}\,\mathrm{Re}\,f(\eta)\theta'(\eta)+\mathrm{Pr}\,\mathrm{Re}\,Q\theta(\eta)=0. \quad \text{... (13)}$$

$$\phi''(\eta)+Sc\,\mathrm{Re}\,\phi'(\eta)f(\eta)-Sc\,\mathrm{Re}\,Kr(1+\Lambda\theta(\eta))^m\phi(\eta)e^{\frac{-E}{1+\Lambda\theta}}=0. \quad \text{... (14)}$$

where $A_1=\mu_{Nf}\left(\mu_f\right)^{-1}$, $A_2=\rho_{Nf}\left(\rho_f\right)^{-1}$, $A_3=k_{nf}\left(k_f\right)^{-1}$, $A_4=\left(\rho C_p\right)_{Nf}\left[\left(\rho C_p\right)_f\right]^{-1}$

and the Eq. (7) and (8) returns

$$f=0, f'=1, g=0, \theta=1, \phi=1 \text{ at } \eta=0. \quad \text{... (15)}$$

$$f=Sp, f'=0, g=0, \theta=0, \phi=0 \text{ at } \eta=1. \quad \text{... (16)}$$

The Wall shear stress, Nusselt and Sherwood number are defined as follows

$$C_{fx} = \frac{A_1}{A_2}(1+\lambda) f''(0)$$

$$Nu_x = -(A_3 + Rd)\ \theta'(0)$$

$$Sh_x = -\phi'(0)$$

Numerical methodology

The solutions of a nonlinear coupled system of equations Eqs (11)-(14) with (15) and (16) are very tedious by applying the analytical method. The shooting technique and the Runge-Kutta method were utilized to address this obstacle. MATLAB software is used to program this procedure, and the results are explained using graphs in the following sections. Additionally, previously published results are used to validate our findings. We chose 0.01 for the step length and 10^{-6} for the convergence tolerance for all of the numerical processes, We set η values such that the boundary criteria (i.e., conditions $\eta = 0$ and $\eta = 1$) are satisfied.

A detailed description of the numerical procedure of the shooting method along the R-K-F scheme is given below. First to set up the initial variables for transforming non-linear ODE into the first-order system of differential equations: $x(1) = f;$

$x(2) = f'; x(3) = f''; x(4) = f'''; x(5) = g;$

$x(6) = g'; x(7) = \theta;\ x(8) = \theta';\ x(9) = \phi;\ x(10) = \phi'.$

Numerical Algorithm:

$x'(1) = x(2);$

$x'(2) = x(3);$

$x'(3) = x(4);$

$x'(4) = f^{iv};$

$x'(5) = x(6);$

$x'(6) = g'';$

$x'(7) = x(8);$

$x'(8) = \theta'';$

$x'(9) = x(10)$

$x'(10) = \phi''$

Where

$$f^{iv} = \frac{(1+\lambda)A_2}{A_1}\left\{\left(\mathrm{Re}\left[x(2)x(3) - x(1)x(4)\right]\right) - 2Rp\ x(6) + \left(\frac{M^2}{A_2} + \frac{KA_1}{A_2}\right)x(3)\right\}.$$

$$g'' = (1+\lambda)\frac{A_2}{A_1}\left\{\left(\mathrm{Re}\left[x(1)x(6) - x(1)x(5)\right]\right) - 2Rp\ x(2) + \left(\frac{M^2}{A_2} + \frac{A_1 K}{A_2}\right)x(5)\right\}$$

$$\theta'' = \frac{-1}{A_3 + Rd}\left\{A_4 \Pr \mathrm{Re}\, x(1)\ x(8) + \Pr \mathrm{Re}\, Q\ x(7)\right\}.$$

$$\phi'' = -Sc\,\mathrm{Re}\, x(10)x(1) + Sc\,\mathrm{Re}\, Kr(1+\Lambda\ x(7))^m\, x(9) e^{\frac{E}{1+\Lambda\ x(7)}}.$$

with boundary conditions: $x(1) = 0; x(2) = 1; x(5) = 0; x(7) = 1; x(9) = 1$ at $\eta = 0$ and $x(1) = Sp; x(2) = 0; x(5) = 0; x(7) = 0; x(9) = 0$ at $\eta = 1$

Results and Discussion

The study focuses on examining the heat and mass transfer phenomena of a Jeffrey nanofluid utilizing the Tiwari-Das model within a rotating channel incorporating activation energy. Graphical representations illustrating the effects of various physical parameters on the velocity field, fluid temperature and concentrations, skin friction coefficient, Nusselt & Sherwood Numbers and streamlines are presented in Figs 2-22.

Velocity Profiles

The effect of the magnetic field and injection parameter on velocity profiles for *x*-, and *y*-directions is represented in Figs. 2 and 3. In Fig. 2, velocity falls

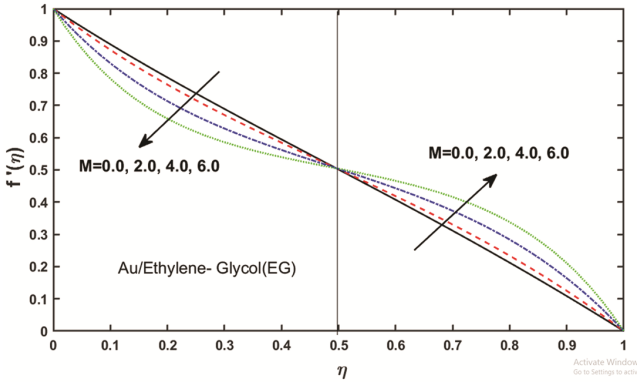

Fig. 2 — Impact of *M* on $f'(\eta)$

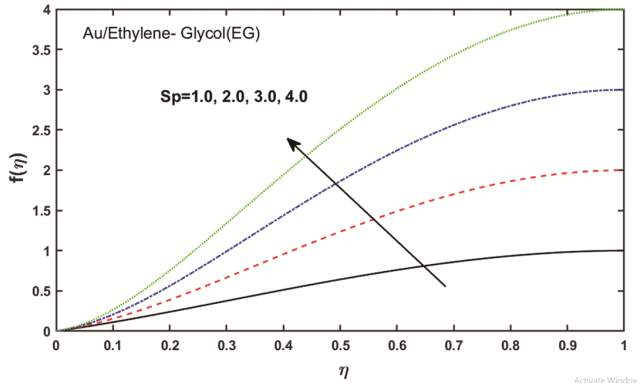

Fig. 3 — Impact of *Sp* on $f(\eta)$

in $0 \le \eta \le 0.5$ and the opposite trend is found in the remaining M values such as $0.5 \le \eta \le 1$. The low velocity is due to the Lorentz drag force, which is generated by the magnetic parameter and restricts particle motion. Consequently, this increases the thickness of the boundary. Moreover, as demonstrated in Fig. 3, the velocity profiles rise as the injection parameter increases.

Figs 4-7 illustrate the outcomes of Jeffrey, rotation, permeability parameter, and Reynolds number on transverse velocity profiles. As the value of the Jeffrey fluid in Fig. 4 increases, the velocity distribution improves. The increase in the Jeffrey fluid parameter promotes more efficient fluid flow by enhancing the elasticity of the fluid, reducing energy dissipation, and consequently increasing fluid velocity. For greater values of the spinning parameter *Rp*, the fluid's momentum increases which is represented in Fig. 5. The velocity profiles rise as the rotation parameter is raised due to an increase in the Coriolis force. Fig. 6 illustrates that as permeability rises, the velocity field decreases. The decrease in fluid velocity with an increase in permeability is due to the combined effects of reduced flow resistance and increased fluid retention within the porous medium. Fig. 7, It observed that transverse velocity declines when for Reynolds number goes up. It demonstrates the relative importance of gravitational forces to viscous forces in the fluid flow, which makes velocity boundary layer thicknesses decrease as the Reynolds number goes up.

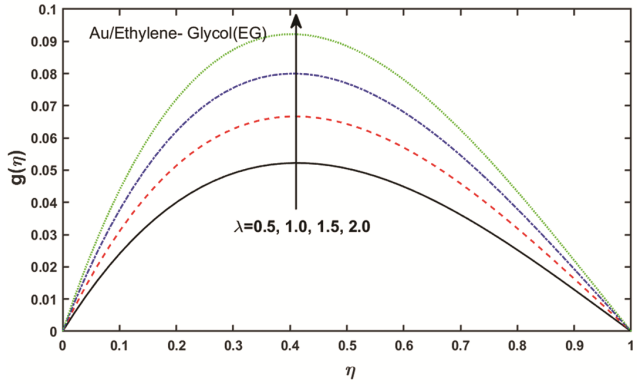

Fig. 4 — Impact of λ on $g(\eta)$

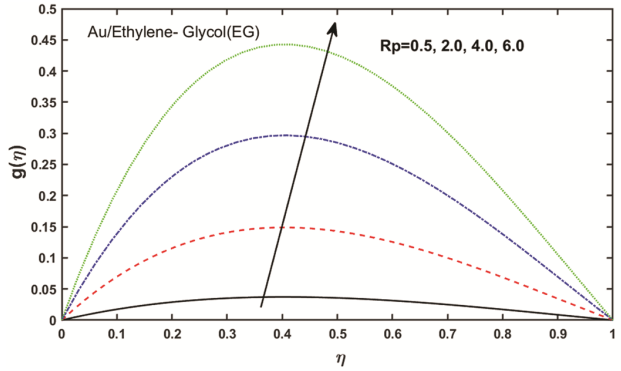

Fig. 5 — Impact of *Rp* on $g(\eta)$

Temperature Profiles

The effects of Jeffrey parameter λ, *Rd, M*, *Q*, and Re on temperature profiles are illustrated in Figs 8 -12. As illustrated in Fig. 8, it has been

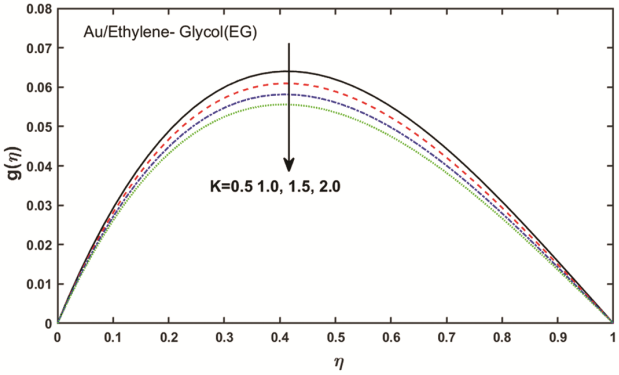

Fig. 6 — Impact of *K* on $g(\eta)$

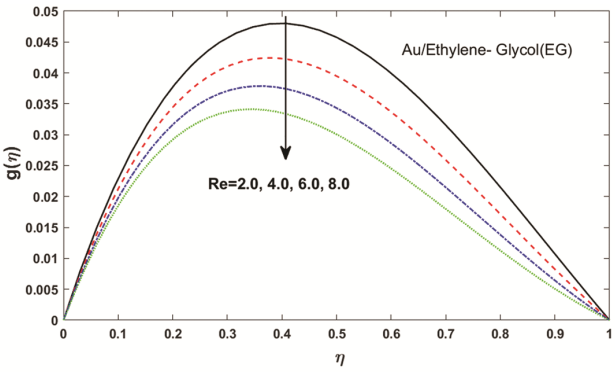

Fig. 7 — Impact of *Re* on $g(\eta)$

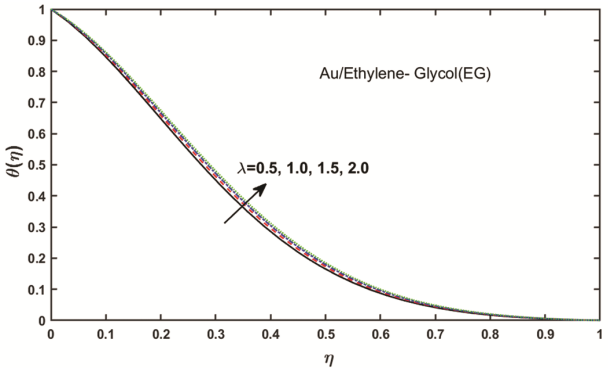

Fig. 8 — Impact of λ on $\theta(\eta)$

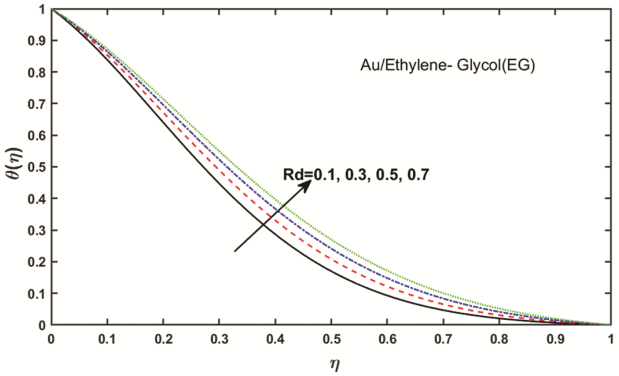

Fig. 9 — Impact of *Rd* on $\theta(\eta)$

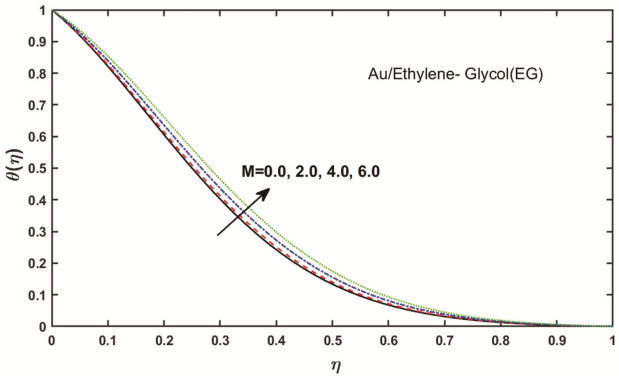

Fig. 10 — Impact of *M* on $\theta(\eta)$

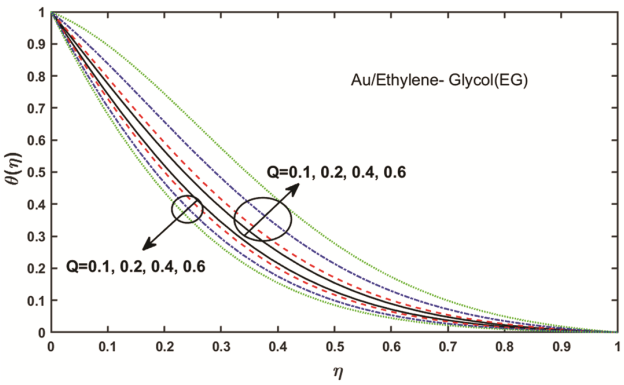

Fig. 11 — Impact of Q on $\theta(\eta)$

determined that the temperature distribution increases as the amount of Jeffrey fluid increases. The increase in fluid temperature with an increase in the Jeffrey fluid parameter is a result of the altered heat transfer properties of the fluid due to its increased elasticity, which affects both heat dissipation and thermal energy storage within the fluid. From Fig. 9 it can be seen that when *Rd* increases, the temperature field improves. The increase in the radiation parameter

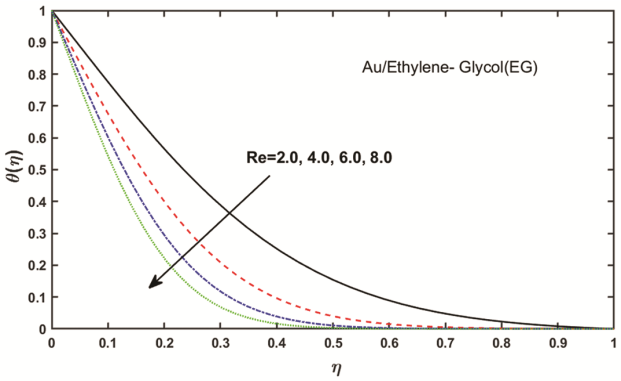

Fig. 12 — Impact of *Re* on $\theta(\eta)$

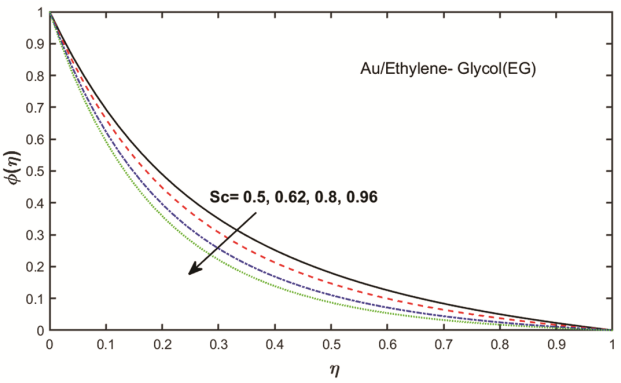

Fig. 13 — Impact of *Sc* on $\phi(\eta)$

leads to a higher influx of radiant energy into the fluid, which increases the kinetic energy of its molecules and results in a corresponding increase in fluid temperature. The impact of M on dimensionless temperature is shown in Fig. 10. As the magnetic parameter is increased, the fluid's temperature rises. Fig. 11 shows how Q affects the temperature profile. The fluid temperature is shown to rise as the heat-generating parameter rises and falls as the heat-sink parameter rises. The increase in the heat source parameter leads to a higher rate of heat input into the fluid, which results in an increase in its temperature due to the additional thermal energy supplied to the system. As shown in Fig. 12, the temperature profile decreases as the Reynolds number increases.

Concentration Profiles

It is obvious from Fig. 13 that the diffusivity drops as the *Sc* increases. When *Sc* increases, the fluid's mass diffusivity decreases, resulting in a lower particle concentration. A similar trend has been noted in Fig. 14 with the chemical parameter rising. Due to its consumption in the reaction, chemical molecule

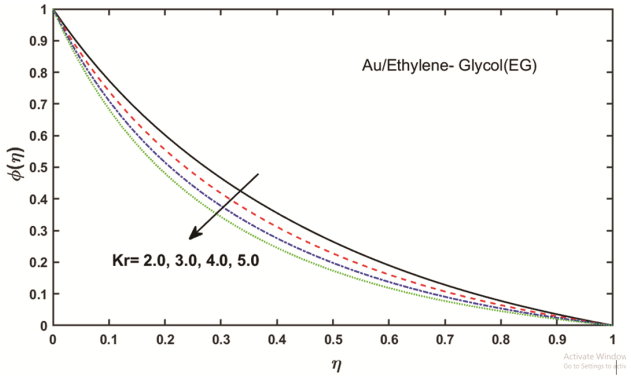

Fig. 14 — Impact of *Kr* on $\phi(\eta)$

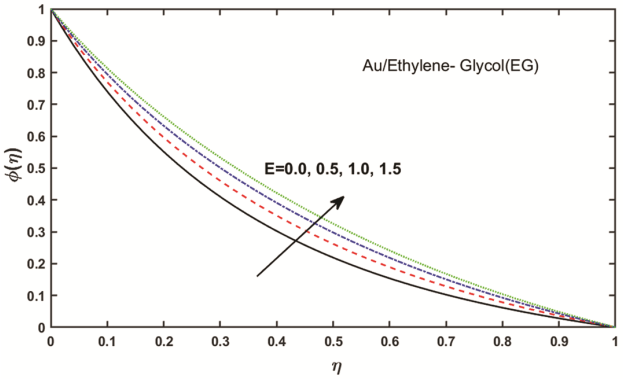

Fig. 15 — Impact of *E* on $\phi(\eta)$

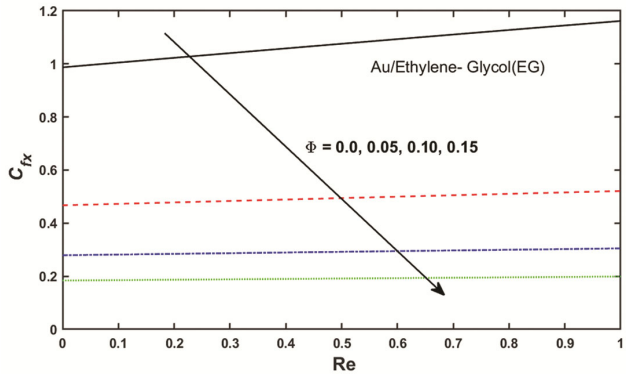

Fig. 16 — Impact of Φ on C_{fx} against *Re*

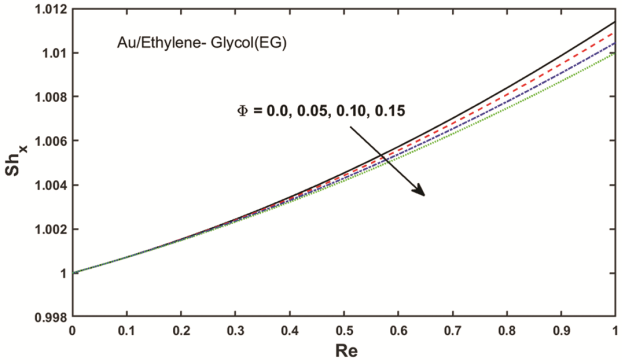

Fig. 17 — Impact of Φ on S_{hx} against *Re*

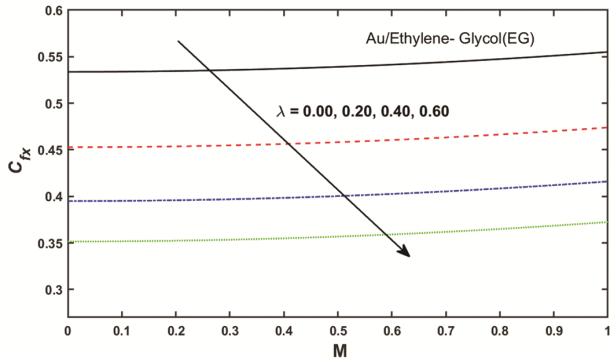

Fig. 18 — Impact of λ on C_{fx} against *M*

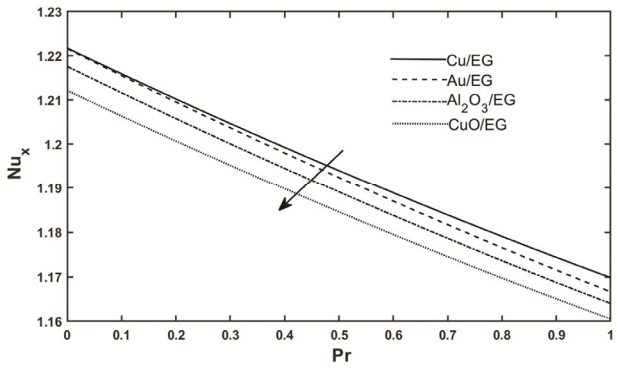

Fig. 19 — Impact of different nanoparticles (Cu, Au, Al_2O_3, CuO /*EG*) on Nu_x against *Pr*

diffusivity decreases with increasing *Kr*. Consequently, fluid concentration decreases. It is noticed that the species concentration increases as Arrhenius energy increases from Fig. 15. As the activation energy value increases, the Arrhenius function decreases, thereby facilitating generative chemical processes that enhance concentration.

Skin-friction coefficient, Nusselt & Sherwood number profiles

Figs 16 and 17 depict the friction coefficient and Sherwood number in relation to the *Re* against Φ. The friction factor and Sherwood numbers were observed to decrease as the volume fraction parameter value increased. From Fig. 18, it is shown that the wall shear stress decreases with rising values of the Jeffrey parameter.

Fig. 19 portrays the characteristics of Nusselt number for various nanoparticles such as *Cu*, *Au*, Al_2O_3 and *CuO*. It is noticed that the heat transmission rate is high in *Cu-EG* nanofluid compared with *Au-*

EG, Al_2O_3-*EG* and *CuO-EG* in order. The heat transfer rate for *CuO-EG* seems low. Further, it is monitored that the heat transfer rate declines sharply for growing values of volume fraction of the nanoparticles and the Prandtl number.

Validation

In order to authenticate the precision of the outcomes, the computational values of $f'(\eta)$ and $\theta(\eta)$ are figured (Figs. 20-21) for various values of *Re* and *Pr* and compared with previously published results by Sheikholeslami *et al.*[37], Vajravelu *et al.*[38], and Mehbood *et al.*[39] exceptional agreement between the results is seen in the Figures. From this, it follows that the comparison validates the accuracy of the numerical method and the final results. Table 1 demonstrates the Nanofluid's thermophysical characteristics and Table 2 demonstrates the Thermophysical characteristics of *EG* as base liquid and Gold, copper, Aluminium oxide and Copper oxide (*Au*, *Cu*, Al_2O_3, and *CuO*) *as* nanoparticles.

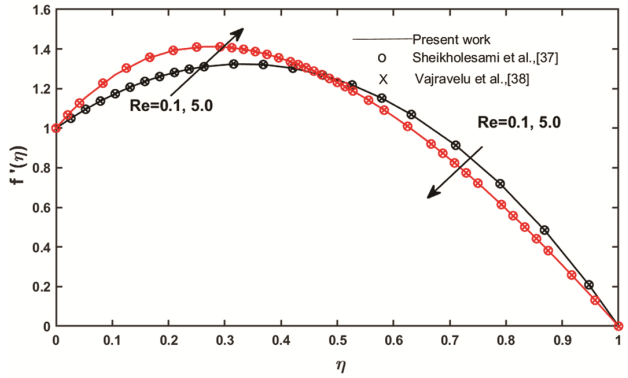

Fig. 20 — Comparison of $f'(\eta)$ between present work and published literature

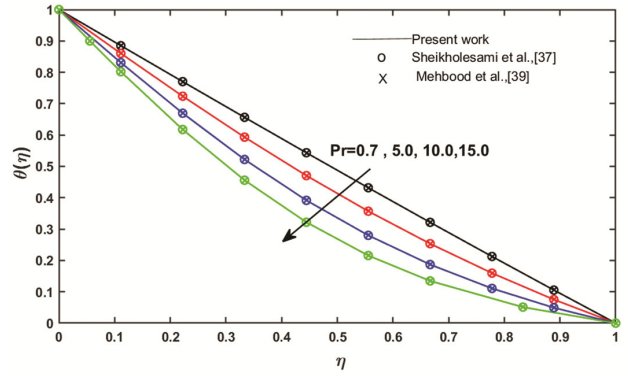

Fig. 21 — Comparison of $\theta(\eta)$ against *Pr* between present work and Sheikholeslami *et al.*[37] & Mehbood *et al.*[38]

Streamline analysis

Fig. 22((a) &(b)) depicts the stream function defined by Eq. (9) for various values of injection parameter (*Sp*). It is found that the behaviour of the streamlines for Sp=0.3 is substantially more robust than *Sp*=0.5.

Table 1 — Thermophysical characteristics of the nanofluid

Properties	Nanofluid
Density	$\rho_{Nf} = \Phi\rho_s + (1-\Phi)\rho_f$
Viscosity	$\mu_{Nf} = \frac{\mu_f}{(1-\Phi)^{2.5}}$
Thermal conductivity	$\frac{k_{Nf}}{k_s + 2k_f - 2\Phi(k_f - k_s)} = \frac{k_f}{k_s + 2k_f + \Phi(k_f - k_s)}$
Heat capacity	$(\rho C_p)_{Nf} = \Phi(\rho C_p)_s + (1-\Phi)(\rho C_p)_f$

Table 2 — Thermophysical characteristics of *EG* as base liquid and gold (*Au*), copper (*Cu*), aluminium oxide (Al_2O_3), and copper oxide (*CuO*) nanoparticle

Physical properties	*Au*	Al_2O_3	*CuO*	*Cu*	*EG*
$k(W/mK)$	318	40.0	18	401	0.252
$C_p(J/kgK)$	129	765	540	385	2415
$\rho(kg/m^3)$	19300	3970	6510	8933	1114.0

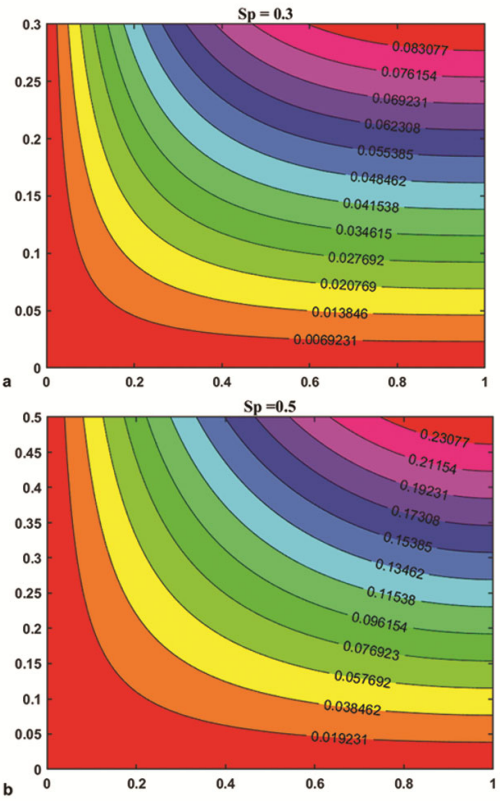

Fig. 22 — Variation of streamlines for different values of *Sp*

Conclusion

This problem examines the study of the heat and mass transfer effects of Jeffrey nanofluid using the Tiwari Das model in a revolving channel containing activation energy. Graphical representations of the consequences of different physical parameters on the velocity field and fluid temperature are provided. Key findings from this investigation include:

- The fluid velocity declines sharply for increasing values of the magnetic parameter (*M*) and Reynolds number (*Re*).
- For larger values of the Rotation and the Jeffrey fluid parameters, the velocity field exhibits a sharp rise.
- The dimensionless temperature rises with an increase in the Radiation parameter, Magnetic parameter, and Jeffrey parameter and a reverse tendency has been observed on increasing Reynolds number.
- The concentration profile demonstrates an apparent increase with escalating Arrhenius energy; however, a contrasting trend emerges with a higher Schmidt number and chemical reaction parameter.
- The skin friction coefficient and mass transfer rate decline sharply with an increase in the volume fraction of the nanoparticles.
- The rate of heat transfer diminishes as the Prandtl number and volume fraction of the nanoparticles increase.
- Nusselt number is high for *Cu-EG* nanoparticles due to high specific heat.

These findings showcase their potential to improve heat transfer efficiency across diverse applications including thermal management, materials processing industries, biomedical fields, energy conversion systems, and industrial sectors. The future scope of this research work aims to further enhance the study of ternary nanofluids, potentially leading to significant contributions in research, industry, and society.

Nomenclature

a, A	dimensionless constants
B_0	magnetic field strength
c	concentration distribution
C_p	specific heat at constant Pressure
C_{fx}	skinfriction coefficient
D	diffusion coefficient
$E = \frac{E_a}{kT_h}$	activation energy
f, g	similarity functions of velocity in *x*- ,*y*- directions respectively
h	distance between the plates
$K = \frac{\vartheta_f}{ak_0}$	permeability parameter
$Kr = \frac{h^2 kr^2}{\vartheta}$	chemical reaction parameter
$M = \frac{\sigma_f B_0^2}{\rho_f a}$	magnetic field parameter
Nu_x	Nusselt number
$\Pr = \frac{C_p \mu_f}{k_f}$	Prandtl number
$Q = \frac{hQ_o}{(\rho c_p)_f}$	heat source/sink parameter
$\mathrm{Re} = \frac{ah^2}{\vartheta_f}$	Reynolds number
$Rd = \frac{4T_h^3 \sigma^*}{3k^* k_f}$	radiation parameter
$Rp = \frac{h^2 \Omega}{\vartheta_f}$	spinning parameter
$Sc = \frac{\vartheta}{D}$	Schmidt number
Sh_x	Sherwood number
$Sp = \frac{v_0}{ha}$	dimensionless suction/ injection parameter
T	temperatures distribution
T_0, T_h	temperatures at the lower and upper plates
u, v, w	velocity components along *x*,*y*,*z* axes, respectively
Greek symbols:	
α	thermal diffusivity
Ω	Constant rotation velocity
$\Lambda = \frac{T_0 - T_h}{T_h}$	temperature difference parameter
ρ	Density
λ	Jeffrey parameter
ϕ	Dimensionless Concentration
ϑ	Kinematic velocity
σ	Electrical Conductivity
θ	Dimensionless temperature

Φ	Nanoparticle volume fraction
Subscripts	
f	base fluid
o	cold
h	hot
Nf	Nanofluid
s	Nano-solid-particles
Superscript	
′	primes denote differentiation with respect to η

References

1 Poply V & Vinita K, Analysis of outer velocity and heat transfer of nanofluid past a stretching cylinder with heat generation and radiation, *Proc Int Conf Trends Comput Cogn Eng*, 1169 (2021) 215.

2 Sheikholeslami M & Ganji D D, Numerical investigation for two phase modeling of nanofluid in a rotating system with permeable sheet, *J Mol Liq*, 194 (2014) 13.

3 Rashidi M M, Abelman S & Freidoonimehr N, Entropy generation in steady MHD flow due to a rotating porous disk in a nanofluid, *Int J Heat Mass Transf*, 62 (2013) 515.

4 Ellahi R, The effects of MHD and temperature dependent viscosity on the flow of non-Newtonian nanofluid in a pipe: Analytical solutions, *Appl Math Model*, 37 (2013) 1451.

5 Ali A, Yasir A, Kumam P, Khan B, Adeel A & Zahir S, Flow of a nanofluid and heat transfer in channel with contracting/expanding walls, *IEEE Access*, 7 (2019) 102427.

6 Santhosh N & Sivaraj R, Analysis of mixed convective-radiative heat transfer in a porous square cavity filled with various nanofluids, *Numer Heat Transf Part A: Appl*, (2023) 1.

7 Vijayalakshmi P & Sivaraj R, Heat transfer analysis on micropolar alumina-silica-water nanofluid flow in an inclined square cavity with inclined magnetic field and radiation effect, *J Therm Anal Calorim*, 148 (2023) 473.

8 Sharma K, Kumar S & Vijay N, Insight into the motion of water-copper nanoparticles over a rotating disk moving upward/ downward with viscous dissipation, *Int J Mod Phys*, B36 (2022) 2250210.

9 Kumar S, Sharma K, Makinde D O, Joshi V K & Saleem S, Entropy generation in water conveying nanoparticles flow over a vertically moving rotating surface: Keller box analysis, *Int J Numer Meth Heat Fluid Flow*, 34 (2024) 608.

10 Santhosh N & Sivaraj R, Comparative heat transfer performance of hydromagnetic mixed convective flow of cobalt-water and cobalt-kerosene ferro-nanofluids in a porous rectangular cavity with shape effects, *Eur Phys J Plus*, 138 (2023) 240.

11 Sharma K & Kumar S, Impacts of low oscillating magnetic field on ferrofluid flow over upward/downward moving rotating disk with effects of nanoparticle diameter and nanolayer, *J Magn Magn Mater*, 575 (2023) 170720.

12 Madiha T K & Satya P V N, Impact of Catteno-christov heat flux on mixed convective flow of a ternary hybrid (Cu-Al_2O_3-TiO_2/H_2O) nanofluid over an elongated sheet: A comparitive analysis, *Indian J Chem Technol*, 31 (2024) 57.

13 Sumithra A, Sivaraj R, Ramachandra P V, Anwar-Bég O , Leung H H, Kamalov F, Kuharat S & Rushi K B, Computation of inclined magnetic field, thermophoresis and Brownian motion effects on mixed convective electroconductive nanofluid flow in a rectangular porous enclosure with adiabatic walls and hot slits, *Int J Mod Phys B*, 2450398 (2023) 1.

14 Bestman A R, Natural convection boundary layer with suction and mass transfer in a porous medium, *Int J Energy Res*, 14 (1990) 389.

15 Khan S U, Waqas H, Shehzad S A & Imran M, Theoretical analysis of tangent hyperbolic nanoparticles with combined electrical MHD, activation energy and Wu's slip features: A mathematical model, *Phys Scr*, 94 (2019) 125211.

16 Muhammad T, Waqas H, Khan S A, Ellahi R & Sait S M, Significance of nonlinear thermal radiation in 3D Eyring–Powell nanofluid flow with Arrhenius activation energy, *J Therm Anal Calorim*, 143 (2020) 929.

17 Khan S U, Tlili I, Waqas H & Imran M, Effects of nonlinear thermal radiation and activation energy on modified second-grade nanofluid with Cattaneo-christov expressions, *J Therm Anal Calorim*, 143 (2020) 1175.

18 Gireesha B J, Archana M , Mahanthesh B & Prasannakumara B C, Exploration of activation energy and binary chemical reaction effects on nano Casson fluid flow with thermal and exponential space-based heat source, *Multidiscip Model Mater Struct*, 15 (2018) 227.

19 Maleque K A, Effects of binary chemical reaction and activation energy on MHD boundary layer heat and mass transfer flow with viscous dissipation and heat generation/absorption, *ISRN Therm*, 9 (2013) 284637.

20 Javed M, Alderremy A A & Farooq M, Analysis of activation energy and melting heat transfer in MHD flow with chemical reaction, *Eur Phys J Plus*, 134 (2019) 256.

21 Shahid A, Huang H L, Khalique C M & Bhatti M M, Numerical analysis of activation energy on MHD nanofluid flow with exponential temperature dependent viscosity past a porous plate, *J Therm Anal Calorim*, 143 (2021).

22 Ibrahim M G & Abou-zeid M Y, Influence of variable velocity slip condition and activation energy on MHD peristaltic flow of Prandtl nanofluid through a non-uniform channel, *Sci Rep*, 12 (2022) 18747.

23 Vajravelu K, Sreenadh S, Lakshminarayana P & Sucharitha G, The effect of heat transfer on the nonlinear peristaltic transport of a Jeffery fluid through a finite vertical porous channel, *Int J Biomath*, 9 (2008) 1650023.

24 Naidu K K & Sreenadh S, The Flow of a Jeffrey fluid in a composite horizontal channel partially filled with a deformable porous material, *Heat Transf*, 52 (2022) 2017.

25 Sreenadh S, Rashidi M M, Kumaraswamy Naidu K & Parandhama A, Free convection flow of a Jeffrey fluid through a vertical deformable porous stratum, *J Appl Fluid Mech*, 9 (2016) 2391.

26 Selvi R K & Muthuraj R, MHD oscillatory flow of a Jeffrey fluid in a vertical porous channel with viscous dissipation, *Ain Shams Eng J*, 9 (2018) 2503.

27 Santhosh N & Radhakrishnamacharya G, Jeffrey fluid flow through porous medium in the presence of magnetic field in narrow tubes, *Int J Eng Math*, 2014 (2014) 713831.

28 Hayat T, Aziz A, Muhammad T & Alsaedi A, Active and passive controls of Jeffrey nanofluid flow over a nonlinear stretching surface, *Res Phys*, 7 (2017) 4071.

29 Shahzad F, Sagheer M & Hussain S, Numerical simulation of magneto hydrodynamic Jeffrey nanofluid flow and heat transfer over a stretching sheet considering Joule heating and viscous dissipation, *AIP Adv*, 8 (2018) 065316.

30 Babu D H & Narayana P V S, Joule heating effects on MHD mixed convection of a Jeffrey fluid over a stretching sheet with power law heat flux: A numerical study*, J Magn Magn Mater*, 412 (2016) 185.

31 Zeeshan A & Majeed A, Heat transfer analysis of Jeffery fluid flow over a stretching sheet with suction/injection and magnetic dipole effect, *Alex Eng J*, 55 (2016) 2171.

32 Nabwey H A, Mushtaq M, Nadeem M, Ashraf M, Rashad A M, Alshber S I & Hawsah M A, Note on the numerical solutions of unsteady flow and heat transfer of Jeffrey fluid past stretching sheet with soret and dufour effects, *Mathematics*, 10 (2022) 4634.

33 Qasim M, Heat and mass transfer in a Jeffrey fluid over a stretching sheet with heat source/sink, *Alex Eng J*, 52 (2013) 571.

34 Kumaraswamy N K, Babu D H, Reddy S H & Satyanarayana P V, Radiation and partial slip effects on magnetohydrodynamic Jeffrey nanofluid containing gyrotactic microorganisms over a stretching surface, *J Therm Sci Eng Appl*, 13 (2021) 031011.

35 Hayat T, Qayyum S, Imtiaz M & Alsaedi A, Melting heat transfer and induced magnetic field effects on flow of water based nanofluid over a rotating disk with variable thickness, *Appl Math Mech Eng Ed*, 39 (2018) 1618.

36 Tiwari R K & Das M K, Heat transfer augmentation in a two-sided lid-driven differentially heated square cavity utilizing nanofluids, *Int J Heat Mass Transf*, 50 (2007) 2002.

37 Sheikholeslami M, Ashorynejad H R, Domairry G & Hashim I, Flow and heat transfer of Cu-water nanofluid between a stretching sheet and a porous surface in a rotating system*, J Appl Math*, 18 (2012).

38 Vajravelu K & Kumar B V R, Analytical and numerical solutions of a coupled non-linear system arising in a three-dimensional rotating flow*, Int Non-Linear Mech*, 39 (2004) 13.

39 Mehmood A & Ali A, Analytic solution of three-dimensional viscous flow and heat transfer over a stretching flat surface by homotopy analysis method*, J Heat Transf*, 130 (2008) 121701.